QATAR UNIVERSITY

COLLEGE OF ARTS AND SCIENCES

ELECTRODE SUSPENSION FOR AQUEOUS SODIUM FLOW BATTERY

BY

MENTALLAH MOHAMED HASSANIN MOHAMED HASSANIN MESLAM

A Thesis Submitted to

the College of Arts and Sciences

in Partial Fulfillment of the Requirements for the Degree of

Master of Science in Material Science and Technology

January 2022

COMMITTEE PAGE

The members of the Committee approve the Thesis of
Mentallah Meslam defended on [Defense Date].

Dr. Ahmed Elzatahry
Thesis/Dissertation Supervisor

Dr. Mohamed Youssry Abdelnaby
Committee Member

Dr. Talal Altahtamouni
Committee Member

Approved:

Ahmed Elzatahry, Dean, College of Arts and Sciences

ABSTRACT

MESLAM, MENTALLAH, M., Master: 2021, Material Science and Technology

Title: ELECTRODE SUSPENSION FOR AQUEOUS SODIUM FLOW BATTERY

Supervisor of Thesis: Dr. Ahmed Elzatahry

In the current study, we attempt to formulate and characterize aqueous electrode suspensions (anolytes) composed of carbon black (KB) and sodium titanate ($Na_2Ti_3O_7$; NTO) dispersed in branched micelle solution. The suspensions were characterized by cyclic voltammetry, impedance spectroscopy, rheology, and simultaneous rheo-impedance spectroscopy. The branched micelle solution showed peculiar microstructure with wide working potential of 2.59 V enabled it to be an excellent dispersing medium for conductive KB. Due to excellent wettability, KB dispersions were electrically percolated at low KB content (0.9 wt%) forming a three-dimensional conductive network with significant flexibility enabled them to retain the electrical conductivity under flow. At 1.5 wt% KB, the anolytes could tolerate high load (25 wt%) of NTO without severe rise in the rigidity and conductivity under static and flow modes. Whilst those formulated in the saturated KB dispersions manifested a serious decrease in the conductivity at high load of NTO nanorods.

DEDICATION

A special thanking to my parents, without them, none of my success would be complete.

ACKNOWLEDGMENTS

I would like to thank all the people who supported me during my academic studies in Master. I would like to express my appreciation to my thesis supervisor Dr. Ahmed Elzatahry, who present a great opportunity to do my master thesis under his supervision and for his guidance in carrying out my thesis work.

I would like to express a special thanks to Dr. Mohamed Abdelnaby for being the most supportive person for me during doing my thesis, he acted as a Co-supervisor during my thesis work. I am grateful for all his instructions and assistance that he provide it to me. His patience, vision, and motivation had developed my skills and experience.

Additionally, I would like to thank all faculty members of the Material Sciences and Technology. I really appreciate your effort in teaching me during my study.

TABLE OF CONTENTS

LIST OF FIGURES

CHAPTER 1: INTRODUCTION

1.1 Background

Electrochemical energy storage systems (EESS) including fuel cells [1], supercapacitors [2] and redox batteries [3]. Among different types of EESS, most studies mainly focused on three types of systems such as Redox flow batteries (RFBs) [4], electrochemical flow capacitors (EFCs) [5], and semi-solid flow batteries (SSFBs) [6]. Additionally, an attention is paid to raising alternatives for traditional systems because of their scalability, economical feasibility, environmentally friendly and storage sustainability [7]. As a unified aim, the research and development of EESS have been focused on improve the power and energy densities of these systems for widespread implementation in light-duty vehicles [8] and grid applications [9]. However, there is a lot of factors that affect the efficiency of any EESS such as, the selection of materials for designing composite electrodes [1] and nature of nanostructured materials [10, 11]. Which have been demonstrated to be the key solutions for the challenges encountering the real applications of EESS [1].

Among these, the SSFBs are considering as a promising EESS [6].Where the electrical energy is stored in two different soluble couples [12]. All the liquid materials are stored in external tanks, where they will be pumped by the reactor at which the reaction and the ion exchange occurs [12]. In the SSFBs the total capacity and the energy of such a battery is related to the volume tanks. The SSFBs are classified into two different types; the aqueous and the non-aqueous SSFBs according to the type of electrolyte (dispersed medium) that used in the battery. To our knowledge many work had been done in the non-aqueous SSFBs and few work had been done so far in addressing the rheological and electrical properties of KB dispersions in SSFBs using aqueous medium. However, few studies focused on the modeling design, rheology,

and operation of the flowable electrodes [13-16]. The flowable suspension electrodes mainly consist of conductive materials, electroactive materials (solid particles) which are dispersed in a liquid medium (electrolytes) to form a biphasic dispersion that will be ionically and electrically conductive [17]. During the operation of the flowable electrodes, the slurries are pumped in a polarization cell, and voltage will be applied [17]. Many studies and efforts have been done to develop the materials which are used in the electrochemical systems especially the flowable suspension electrodes [9, 18-20]. Therefore, the focus was on the electrode formulation which should optimally fulfils the following criteria: (i) the active and conductive materials are chemically and physically compatible, (ii) the ratio of solid content and electrolyte and consequently the rheological properties of electrode slurries, and (iii) ratios and protocol of mixing of components [21, 22] for obtaining enhanced electrochemical performance. Carbon nanomaterials (CNMs) are a crucial component in the electrode slurry, which imparts its electronic conductivity due to the formation of extended network of arms, the so-called percolated network. These nanomaterials are marked by peculiar chemical stability, electrical, and mechanical properties of the electrolyte. Among various kinds carbon blacks (CBs) have been commonly used in the formulation of electrodes [10, 23]. Carbon black is a semispherical primary particle of nanometric (few 100 nm) size, which are combine to grow and forms an aggregates in suspensions and in consequence lead to the construction of percolated network formed by branches (pathways) of CB aggregates resulting in three– dimensional network [14]. The surface properties (area and functional groups) of CBs play important role in determining the power of binding forces [24]. Where it helps to determine the microstructure and the flowability of CB suspensions [25]. However, there is a critical concentration (namely; percolation threshold), at which the three

dimensional network is formed within the CB suspension producing severe rise in the mechanical properties (e.g. shear viscosity, shear modulus, and yield stress) [14, 26]. It had been previously reported that the particle size of CBs determine rheological behavior of dispersions where large particles form weak networks composed of lessly compact agglomerates with many pathways that reduce the rheological plateau modules and electrical conductivity [14]. In the current study, we attempt to formulate and (rheologically and electrically) characterize the aqueous anolytes composed of carbon black (conductive additive) and sodium titanate (active material) dispersed in branched micelle solution (dispersing medium). The branched micelle solution was used to extending the working potential window and eventually enhancing the energy density of the electrolytes in sodium semi-solid flow battery.

1.2 State of the problem

Typically, the electrodes of SSFBs are flowable suspensions consist of lithium-based active material and conductive additive dispersed in an organic electrolyte. The current SSFBs encounter some limitations toward real commercialization and performance in large-scale applications due to limited energy density, the environmental impact of organic electrolyte, and high cost of lithium-based materials. Recently, a novel concept, the so-called semi-solid flow batteries (SSFBs), overcomes these limitations and proved to be of significant interest in large-scale storage applications. The current SSFBs rely on the utilization of expensive less abundant lithium-base electrode materials, and KBs dispersed in toxic organic electrolytes.

1.3 Goals and scope

In our study, we aim to formulate and optimize of higher–energy density aqueous suspension electrodes (anolytes) of sodium-based electroactive materials through utilizing: (i) cheap and safe aqueous electrolytes which is an aqueous branched

micelle solution (dispersing medium) that will help to extend the working potential and impart colloidal stability for the electrode suspensions considering this a novel approach to suspension electrodes for aqueous sodium flow batteries, (ii) sodium-based electroactive materials with high capacity.

The outcome of this study is expected to advance the current state-of-the-art semi-solid flow battery through optimizing the composition and operating conditions of environmentally friendly aqueous electrode suspensions of abundant sodium-based materials. This aims to overcome these limitations through optimizing of the composition and operating conditions of aqueous sodium-based electrode suspensions. Aqueous (branched) micelle solution is proposed to be structured dispersing medium that will: (i) enable increasing the content of electroactive materials and extending the working potential window and eventually enhancing the energy density, and (ii) substitute the toxic organic media. Sodium-based active materials will be utilized to replace costly and scarce lithium-based counterparts. However, there are still many key challenges that should be considered to formulate and optimize the composition and operating conditions of these storage systems and many considerations should be tackled to develop the materials used in the electrodes by focusing on improving the electrochemical and rheological performance of flowable electrodes to achieve a flowable aspect of the suspensions which offers flexibility in system design by decoupling the energy and power ratings.

CHAPTER 2. LITERATURE REVIEW AND BACKGROUND

Redox flow cells use electrolytes with electroactive compounds to generate electricity via a reversible reaction. Compared to fuel cells which are dependent on the supply of fuel, flow cells are dependent on electrolytes which are usually stored externally [2]. The electrolytes are divided into catholyte and anolyte which flow through the cathode and anode respectively [5]; the two mix to produce electricity. The electrodes are separated by a membrane which prevents the two electrolytes from mixing in an uncontrolled way and maintains electrical neutrality.

2.1 Redox flow batteries (RFBs)

In 1970s, redox flow batteries (RFBs) showed great interest as an alternative energy storage system that provides reversible conversion between electrical and chemical energy. Thanks to their design flexibility in separating energy and power when compared to solid ion-batteries like lithium-ion batteries [27]. Therefore, this flexibility led to the unique design of the RFB where the energy is stored in two electrolytes that are composed of active materials; namely (anolyte and catholyte) placed in two separated tanks and pumped in a region called the active region where redox reactions occurred [28]. In general, the RFB consists of two electrochemical active components that are dissolved in either aqueous or organic solvents within the specific system and separated by a membrane [28, 29]. Typically, the anolyte solution flows through a porous electrode and reacts to enhance the flow of electrons, which migrate through the external circuit. The charge-carrying species are transferred to a separator, which works to detach the anolyte and catholyte solutions [30]. Therefore, the RFBs are characterized by the concept of having all reactants as an ionic species, where the absence of solid phases and electrolyte circulation allows these types of batteries to have high power capability. Additionally, there are many inconceivable

features for RFBs like, (i) maximizing the capacity by increasing the electrolyte/tank volume slightly; (ii) full discharge as possible without detrimental effects; (iii) the anolytes/catholytes can be used for an infinite time, and (iv) instantons response of the battery (<1 ms) [31].

However, such energy storage systems still provided low energy density (about 40 Wh/L for the fluid alone) due to the limited solubility of active materials (typically 1 – 2 M) and low working potential due to electrolysis [32]. However, many approaches have been done to overcome this obstacle like (i) increasing the solubility of the active materials in the aqueous medium (lithium iodide; 8.2 M) which obtain a yield of 147 Ah/L [27], (ii) using organic active materials which dissolved in nonaqueous media to provide a low energy density of (5-9 Wh/L) with a maximum solubility of (2.6 M), and (iii) using a metal-based electrode as half-cell to assembly hybrid flow battery having an energy density of 550 Wh/L at 8.2 M [33].

As aforementioned that there is a rapid increase in focusing on flow batteries in the field of research, especially the studies that present novel redox couple systems and flow type systems. Recently, metal-or inorganic-based aqueous RFBs have demonstrated a conventional electrochemical performance and have attributed to large-scale field testing at the commercial level. Even though it had been noticed that protic systems have some drawbacks, for example, REBs have low operation potential (<2 V), low energy density (~50 Wh/L), and it showed side reactions in water electrolysis. Therefore, many efforts had been focused on ways of developing new systems to raise the energy density and operating voltage [34].

The electrolyte is the most crucial component in RFBs. Due to their capability to dictate the overall performance of the battery. In general, RFBs are classified into three main types based on the solvent that is used to dissolve the active species, they

are divided into aqueous or non-aqueous RFBs. Based on the structure of the battery itself and the physical state of the active materials which divided them as, all-soluble RFBs, semi-solid RFB, hybrid RFB, and redox–targeting RFBs [29]. As the RFB depends on using two soluble active materials, where interestingly the electrolyte concentration are used to determine the energy density of several systems [34].

In terms of solubility, higher solubility of all redox agents is always desired. Furthermore, the voltage window is one of the major features in RFBs. However, RFBs always possess a limited voltage window of water, especially in the aqueous RFB. Additionally, the viscosity of the electrolyte is another important parameter in RFBs, and it should be low as possible as to provide good electrochemical performance [35]. Madec *et al* attempted to formulate and characterize an optimum electrode suspension for a specific type of RFB and reported the influence of the addition of a surfactant in the composition of the suspension [14]. It was concluded that when the viscosity decreases, the electronic conductivity increases and is less affected by the shear flow, and therefore the electrochemical performance will improve. However, there are still many technical problems that appeared while using RFBs, especially at the commercial level. Among these types of energy storage systems, this work aims to focus on semi-solid flow batteries (SSFBs). Scheme. 1 represents the schematic illustration of a typical SSFB and more details will be discussed about this battery in section (2.2). Therefore, Chiang *et al.* mentioned a new concept, namely semi-solid flow battery (SSFB) which depends on substitute the dissolved ionic species used in RFBs using electroactive solid particles dispersed in a lithium-containing organic electrolyte and mixed up with conductive materials such as percolated carbon blacks [6]. Chiang reported the first SSFB, which demonstrates with Li-ion battery (LIB) materials and SSFBs based on LIB materials showed a high theoretical energy density. But the costs and toxicity

related to their electrolytes are major drawbacks.

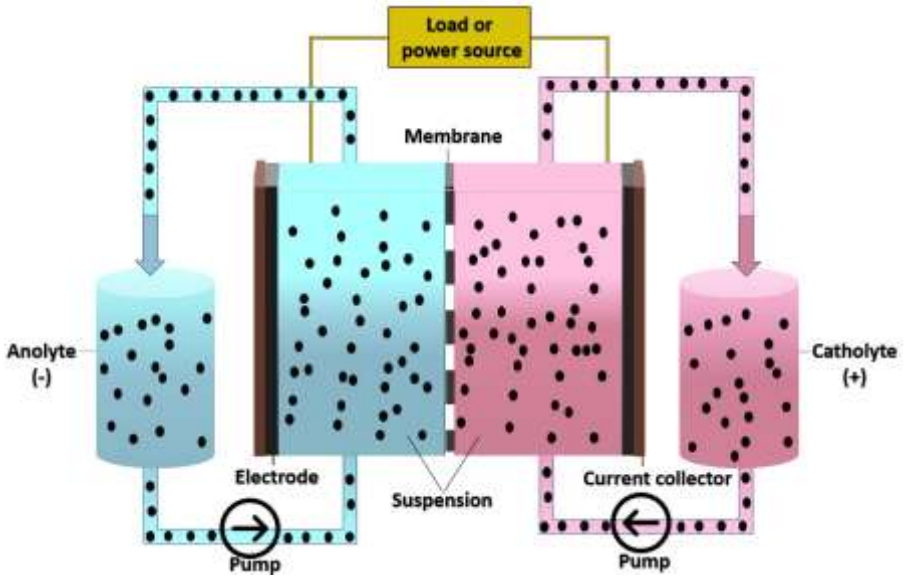

Scheme 1 Typical Semi-solid redox flow battery.

2.2 Semi-solid flow battery (SSFBs)

In SSFBs, the electrode dispersions are consisted of a percolating 3D network that consisted of capable to be electronically conducting and charge storing active particles dispersed in a liquid electrolyte [29]. Therefore, this system provides a higher charge capacity of solid active particles compared to soluble redox systems and allows the energy storage capacity in SSFBs to be 10 times more than that of traditional redox flow batteries [15]. Duduta *et al.* developed the idea of semi-solid flow cell (SSFC), in which traditional liquid electrodes are composed of colloidal suspensions as Li-ion compounds [6]. Also, exchange the traditional stationary current collectors with conductive additives materials in flowable suspensions. Such a flowable suspensions, which consider as an advantage of the Li-ion batteries high energy density in parallel flow batteries design. It is worth to mention that carbon black has a significant role in providing rheological benefit as it is support and creates a electrode slurry.

The percolated conductive network of the carbon black (i.e., Ketjen black,

KB600) is considered a prominent component in the suspension electrodes in the SSFBs. The formation of the 3D network of the CB mainly depends on the particle size, surface area, surface chemistry of CB, and the compatibility of the CB with the dispersing medium. In addition, the percolated network breaks up underflow and sometimes the dispersion loses its conductivity and this may limit the usage of SSFBs [35]. The authors reported that the percolated CB is mainly influenced by the active material content. Hence, they indicated that there is a critical concentration of electronically–insulator active material beyond breaking up of the conductive network or even pathway rupturing may take place and the electrode suspension loses its conductivity.

Additionally, adequate redox potential is desired to reach a high open-circuit voltage (OCV) and high energy density. Nevertheless, aqueous and nonaqueous flow batteries are promising findings in EESS technologies which are capable for achieving the low costs required for widespread implementation [36]. Moreover, the OCV is determined by the electrochemical window of the dispersing medium (electrolyte). To fully optimize and formulate SSFBs, the flowing electrodes should composed of high amount of active material and conductive additives to overcome the resistive nature which occurred from the electrochemically active Li-ion compounds [37]. Nevertheless, as the solid content increases, there would be a dramatic change in the rheological properties, which inhibit flow of the dispersion. Therefore, the key to maximizing the content of the active material while keeping the dispersion yet flowable and conductive is to simultaneously study the respective interactions between all particles that existing within these electrode suspensions [14].

Among various types of anode materials, titanium-based nanomaterials have attracted immense interest in the last decade due to their faster Na ion diffusion,

efficient storage activity, high cycle stability, low operation voltage, low cost, facile synthesis, and environmental issue (Xu *et al.*, 2018). Specifically, sodium titanates ($Na_2Ti_nO_{2n+1}$) have been regarded as potential anode materials after the pioneering work of Senguttuvan and coworkers [31]. Particularly, sodium trititanate ($Na_2Ti_3O_7$) had gained great interest. Although the theoretical capacity of $Na_2Ti_3O_7$ is equal (178 mAh g^{-1}) [38].

Recently, Ventosa *et al.* provided a prototype of Na-ion SSFB containing anolyte and catholyte of Na-based active materials which offered an energy density of *ca.* 9 Wh/L [39]. However, this limited density was ascribed to the large over-potential of suspension electrodes that enhanced by the appropriate selection and optimizing of the electrolyte, active materials, and cycling conditions.

Additionally, there is a great interest in replacing the high-cost toxic organic solvents with aqueous solvents because of the economical, safety and environmental impacts. Even though, the water electrolysis at 1.23 V and possible side reactions minimize the cell voltage. Therefore, the electrode storage compounds should be probably selected to offer potentials compatible with the stability of water at a certain pH.

2.3 Semi-solid flow batteries applications

The electrochemical energy storage systems (EESS) have been already entered in many projects in Qatar such as new tramlines, Qatar Petroleum's Dukhan Oilfield, and traffic signal batteries. Recently, novel concept, the so-called semi-solid flow batteries (SSFBs), overcomes these limitations and proved to be of significant interest in large-scale storage applications. So far, the current SSFBs rely on using expensive less abundant lithium-base electrode materials, and spherical carbon blacks dispersed in toxic organic electrolytes. The outcome of this research project will advance the

current state-of-the-art of promising energy storage semi-solid flow battery by: (i) formulating high-energy density suspension electrodes for novel sodium semi-solid flow battery, (ii) replace the organic solvents by environmentally friendly and less costly aqueous branched micelle solution able to stabilize the suspension electrode, (iii) enhancing the colloidal stability of suspensions (anolytes). This, in turn, might help in overcoming the obstacles facing the commercialization of redox flow batteries by increasing the energy density, and improving the electrochemical performance and safety of batteries.

CHAPTER 3: METHODOLOGY

3.1 Materials

Ketjen black EC600JD (KB; density = 1.90 g cm^{-3}, BET surface area = 1270 m^2 g^{-1}, primary particle size = 34 nm) was a gift from Lion Speciality Chemicals Ltd., Japan), cetylpyridinium chloride monohydrate (CPyCl; purity 99.0 – 102%, molar mass = 358.0 g mol^{-1}, critical micelle concentration at (CMC) = 0.12 mM at 25 °C), titanium (IV) oxide anatase (TiO_2, ≥99%), and anhydrous sodium carbonate (Na_2CO_3, ≥99%), were purchased, from Sigma–Aldrich, USA. Sodium salicylate (NaSal; purity > 99.0 %, molar mass = 160.10 g mol^{-1}) were used as supplied from Surechem Products Ltd., UK.

3.2. Synthesis of sodium titanate

Synthesis of sodium titanate $Na_2Ti_3O_7$ (NTO), as anode material, was done by dry ball milling method (as detailed elsewhere [40]) using a ball-mill from Changsha Tianchuang Powder Technology Co., Ltd, China, equipped by agate jars (50 mL) and balls (diameter = 6 mm). Weighted amounts of Na2CO3 anhydrous (1 mole) and TiO_2 anatase (3 mole) were mechanically activated by milling for 5 h at 500 rpm. The activated mixture were then calcined at 800 °C for 3 h (heating rate = 5 °C min–1) in a tube furnace under air. The synthesized titanates were left to naturally cool down to room temperature before grinding by ceramic mortar and pestle

3.3. Preparation of dispersions

The dispersions of carbon black and electrode suspensions were prepared by ball-milling method. In 25 mL-agate jars, weighted amounts of solid materials (KB and NTO) and micellar solution (R1) were mixed using 5-agate balls (∅ 6 mm), keeping fixed balls-to-materials mass ratio. The milling was conducted at a constant speed (500 rpm) and duration (3 h) at room temperature.

3.4 Characterization techniques

3.4.1 Microscopy

The morphology of materials was investigated by transmission electron microscopy (TEM) from JEOL (100 CX), Japan. The TEM specimens were prepared by dispersing traces of powders in acetone; a drop of dispersion was applied to a grid and then dried in the air before recording the micrographs. A scanning electron microscope (SEM) from FEI Nova NanoSEM equipped with an energy dispersive X-ray (EDX) analyser was used to study the morphology of as-synthesized NTO and electrode suspensions. A small amount of freshly prepared sample was applied to aluminium (or copper) gird and dried in air before recording the micrographs. Optical polarized microscope (Opto-Edu (Beijing) Co., Ltd, China) was used to inspect the dispersions homogeneity and structure.

3.4.2 Crystallinity of materials

A Raman spectrometer from ThermoFisher Scientific (DXR), working at excitation wavelength of 532 nm, was used to investigate the degree of graphitization of carbon nanomaterials and characterize the as-synthesized sodium titanate. The crystalline structure and purity of the as-synthesized sodium titanate were determined by X-ray diffraction (XRD) (Malvern Panalytical Empyrean X-ray diffractometer, UK).

3.4.3 Electrochemical characterization

Electrochemical impedance spectroscopy (EIS) of dispersions and cyclic voltammetry (CV) of dispersing medium and were conducted using a potentiostat/galvanostat (SquidstatTM Plus, Admiral Instruments, USA) at ambient temperature. A three–electrode cell configuration (glassy carbon as a working electrode, Pt/Ti wire as a counter electrode and Ag/AgCl as a reference electrode) was

used to study the electrochemical cyclic voltammetry at 2 mV s^{-1}. The EIS spectra expressed by Nyquist plots were fitted to an equivalent circuit using EC – Lab® software (Biologic, France). The electrical resistivity of dispersions was used to calculate the electrical conductivity considering the geometrical parameters (plate diameter and gap).

3.4.4 Rheology

The rheological properties of dispersions and solutions were carried out using a stress-controlled rheometer (Anton Paar MCR 102) equipped with plate–plate geometry (plate diameter 25 mm, gap 1 mm). All measurements were done at constant temperature 25 °C, controlled by Peltier system. The rheological measurements followed a common protocol as follow: (i) the samples were pre-sheared at 100 s^{-1} for 10 min, then left to relax for 5 min, (ii) the linear viscoelastic region was defined by strain sweep test, (iii) the frequency sweep test at an amplitude (from strain sweep) was recorded, and (iv) the flow curve (viscosity vs. shear rate) was acquired. A step rate test was conducted to simultaneously study the electrical behavior of dispersions at particular shear rates (defined from the flow curve), with waiting time of 15 min at each shear rate.

3.4.5 Rheo-impedance spectroscopy

Simultaneous electrochemical impedance measurements at rest and under shear flow were conducted using the rheometer equipped with a customized copper plate-plate geometry (plate diameter 25 mm, gap 1 mm) connected with the potentiostat as shown in Fig. 1. The EIS spectra were collected at ambient temperature with alternating current (AC) amplitude of 100 mV (the linear regime). All dispersions were treated similarly by an initial pre-shearing at 100 s^{-1} for 10 min followed by a duration of 10 min at rest before starting the step rate test.

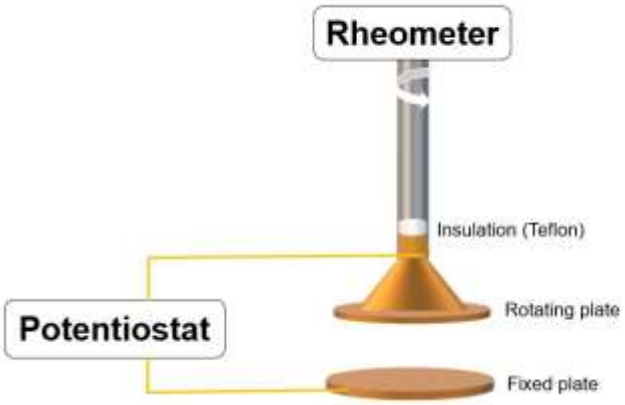

Figure 1 A customized cell for the rheo-electrical study at different shear rates

CHAPTER 4: RESULTS AND DISCUSSION

4.1. Branched micelle solution as an electrolyte

Branched interconnected micelle solution is a peculiar structured phase that is commonly formed in catanionic surfactant system. It is characteristic by its high fluidity, enhanced diffusivity of ions and thermodynamics stability. Among various systems, Cetylpyridinium Chloride (CPyCl) forms a branched micelle system when mixed with sodium Salicylate (NaSal) solution [41], especially at high concentration of NaSal. These unique characteristics render the CPyCl/NaSal solution as an excellent aqueous electrolyte (dispersing medium) for sodium semi-solid flow battery. Moreover, it has been reported that micelle-based electrolytes exhibited excellent electrochemical stability in comparison to common aqueous electrolytes [14] [42].

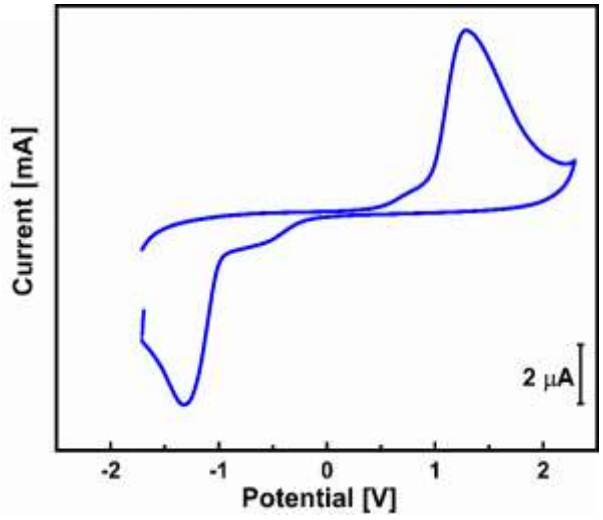

Figure 2 Cyclic voltammogram of the branched micelle solution (0.1 M CPyCl + 0.1 M NaSal) electrolyte, at a scan rate of 10 mVs^{-1}, at ambient temperature.

In this study, various branched micelle solutions of CPyCl/NaSal system (varying CPyCl/NaSal molar ratio) have been examined electrochemically and rheologically. Among them, an optimal solution at 0.1 M CPyCl and 0.1 M NaSal has been selected to be a dispersing medium for electrode formulation. The electrochemical properties of micelle solution has been examined cyclic voltammetry at ambient temperature as depicted in Figure

2. The cyclic voltammogram shows a cathodic peak at 1.29 V and anodic peak at –1.31 V which reveals an extended working potential of 2.59 V. This solution behaves a Newtonian behavior with zero-shear viscosity (η_0) of 350 mPa s at 25 ℃. This relatively low viscosity at higher concentration of Na ion and extended working potential (2.59 V) render the branched micelle solution (0.1 M CPyCl + 0.1 M NaSal) as excellent dispersing medium for the formulation of electrode suspensions.

4.2. Aqueous dispersions of carbon black

The electrode suspension is composed of electrochemical active material and conductive additive dispersed in the electrolyte. Carbon black (keitjen black; KB) has been used as a conductive additive due to its unique characteristics as described in Section 2.2.

Now it is worth to systematically study the rheological and electrical properties of the KB in the selected electrolyte in order to precisely determined the critical content (namely, the percolating threshold) of the KB at which a three-dimensional network is formed.

4.2.1. Rheological properties of carbon dispersions

4.2.1.1. Dynamic strain sweep

Strain sweep test (viz amplitude sweep) is a dynamic rheological test that is done to investigate the alteration of dynamic viscoelastic moduli (G'; storage modulus and G'' loss modulus) with the applied shear strain (γ) at a constant frequency (1 Hz). In general, this is considered as a destructive test that is used to determine the linear viscoelastic region (LVR) that appears over which a minimal disturbance for the microstructure of dispersions is applied. Figure 3a demonstrates strain sweep results for selected KB dispersions at 25 ℃. At KB ≥ 0.3 wt%, the dispersions generally show a gel-like response at low strain where the G' is larger than G'' and both dynamic

viscoelastic moduli are nearly independent of the strain. Above critical strain (γ_c) the KB dispersions exhibit *G′*-*G″* crossover at which the KB dispersions start to behave a liquid-like bahvior where *G″* is higher than *G′* and both moduli decreased with the applied strain. It is worth noting that there is a continuous increase in the dynamic moduli as the concentration of KB increase. For diluted dispersions (KB < 0.3 wt%), *G″* is higher than *G′* and both moduli are independent of γ implying the liquid-like behavior of KB dispersions. As the KB content increases, the *G′*-*G″* crossover shifts to higher γ_c as depicted in Fig. 3b. This behavior can be due to the increased resistivity of the network to the applied deformation as consequence of the increase rigidity of the KB network as carbon content increases. It is rational to note that as the concentration of KB dispersions increase a saturated network of KBs that consist of aggregates are fully constructed with strong bonds and therefore it needs high deformation, so the scaling exponent is a positive value (1.3) implying that the dispersions are composed of stiff saturated networks.

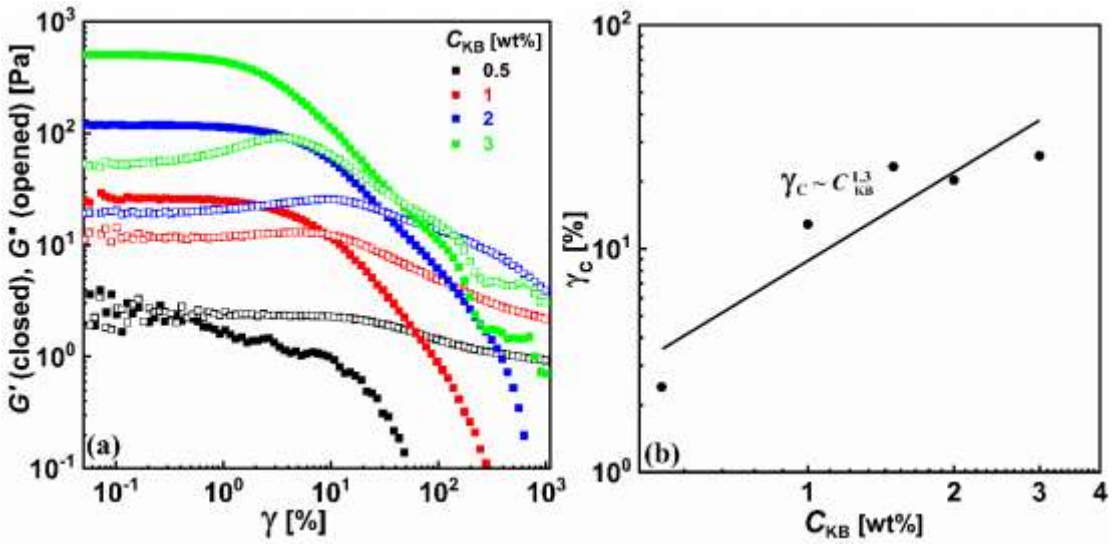

Figure 3 (a) Strain sweep results for selected dispersions of carbon black (KB) in the aqueous electrolyte at 25 °C, and (b) dependency of the critical strain (γ_c) on the carbon black content (C_{KB}).

The variation of the critical strain values (γ_c) on the carbon black content can be ascribed to the network formation which able to resist the deformation that is applied

to the dispersions and the different critical values are related to the nature of the different concentrations of KB dispersions. Hence, these KB dispersions are consists of aggregates that are connected by rigid pathways and are weak enough to broken under deformation during the strain sweep experiment. Obviously, as the concentration of KB dispersions increase a saturated network of KBs that consist of aggregates are fully constructed with strong bonds and therefore it needs high deformation, so the scaling exponent depicted in Fig. 3b is a positive value (1.3) implying that the dispersions are composed of stiff saturated networks [43].

4.2.1.2. Dynamic frequency sweep

The dynamic frequency test is non-destructive one in which a minimal strain (defined from strain sweep) is applied in the LVER, where the microstructure of dispersion is non-perturbed. Therefore, detailed information about the microstructure of dispersions are gained from this test. Fig. 4 shows the frequency sweep results for selected KB dispersions at 25 °C. The diluted dispersions (C_{KB} < 0.3 wt%) display a liquid-like response where G'' is larger than G' and both moduli exhibit dependency on the angular frequency (ω) as shown in Fig. 4a. Upon increasing the KB content at C_{KB} ≥ 0.3 wt%, the dispersions exhibit gel-like response where G' is larger than G'' and both dynamic moduli are somewhat constant with the frequency (Fig. 4b), indicating the formation of structured dispersions. Obviously, the magnitude of the dynamic moduli monotonically increases as the KB content rises. Similar behavior has been shown by analogous carbon nanomaterials in aqueous [26] [44] [45] and organic media [15] [46].

The development of equilibrium microstructure in dispersions can be quantitively monitored from the variation of the plateau modulus (G_0) with the KB content as depicted in Fig. 5.

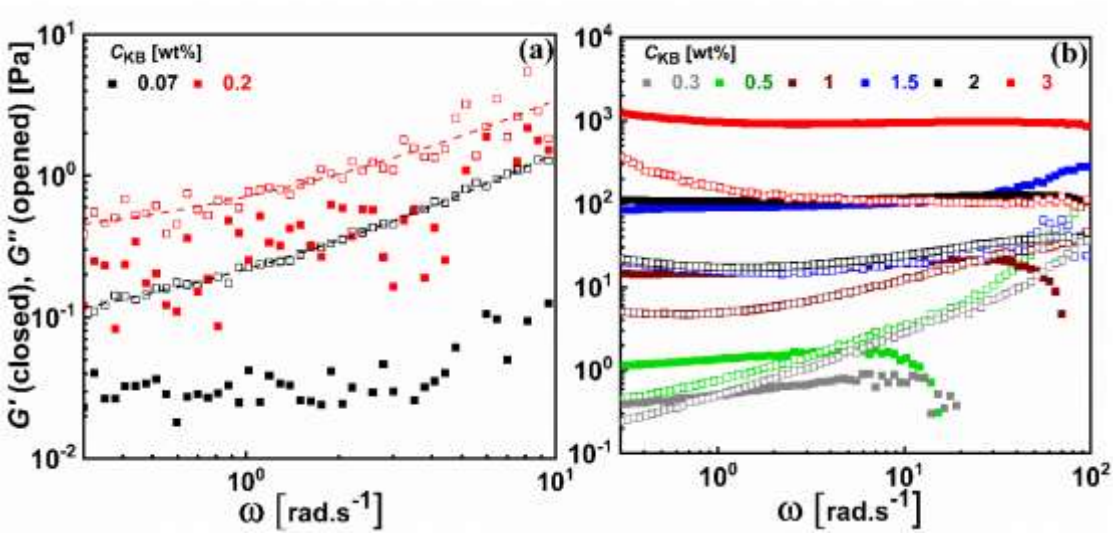

Figure 4 Dynamic frequency sweep results (a) diluted dispersions (strain amplitude = 10%), and (b) concentrated dispersions (strain amplitude ≤ 0.1%) at 25 °C. The dashed lines are guide for eyes.

This modulus is obtained by extrapolating G' to zero frequency from the frequency sweep result, indicating the onset of formation of carbon network in the dispersions (Fig. 5). Such critical content denotes the rheological percolating threshold (C_r*) at which the KB dispersion can be viewed as structured network composed of aggregates that are interconnected through carbon branches. The optical micrograph of the 0.5 wt% KB dispersion (inset of Fig. 5) demonstrates the microstructure of dispersion where a three–dimensional network of carbon is fully constructed at the percolating threshold. Obviously, the plateau modulus monotonically increases with the KB and exhibits a power law relationship: $G_0 \sim C_{KB}^{m}$ with a scaling exponent m = 4.2. This exponent is larger than that has been reported for similar aqueous dispersions [41]. This implies unusual aggregation mechanism of this type of carbon black in the branched micelle solution. Considering the carbon dispersion is composed of flocs (aggregates) connected by branches, the flocs can be treated as uniformly packed fractals [47], where the packing index (D) correlates with the fractal dimension (viz., the scaling exponent m) by equation (1) [48]:

$$D = 3 - \left(\frac{2}{m}\right) \quad (1)$$

The dispersions of KB in the branched micelle solution show a packing index D of *ca.* 2.5 implying a rapid–aggregation mechanism controls by particle – particle aggregation that results in compact structure. Previous studies reported a packing index of 2.7 for nonaqueous dispersions for nonaqueous dispersions [49] and of carbon nanofibers (CNFs) [43].

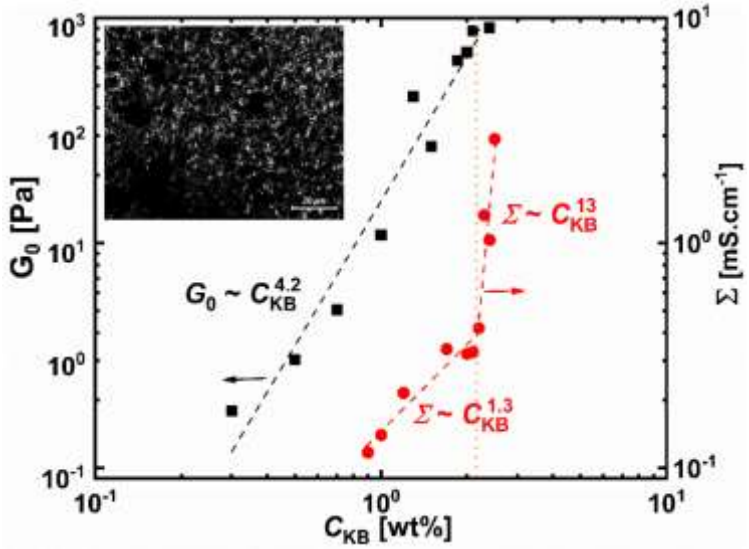

Figure 5 Variation of plateau modulus (G_0) and electrical conductivity (Σ) with the concentration of KB (C_{KB}) at 25 °C. The inset is the optical micrograph of the dispersion at 0.5 wt% KB; the scale bar is 20 μm.

It is worth mentioning the sensitivity of the rheological properties of dispersions to the properties of carbon black (viz. surface area, surface chemistry, shape and size of particles) and the nature of the dispersing medium [50]. Importantly, the compatibility between KB and micellar solution plays a crucial role in controlling the aggregation mechanism and hence the microstructure of dispersion. Indeed, the KB is highly hydrophobic particles which are expected to rapidly flocculate in aqueous medium and shows low percolating threshold. Nevertheless, the branched micelle solution delineates the aggregation mechanism in a way that the microstructure is built by

particle–particle (rather than aggregate–aggregate) mechanism. In comparison, it was mentioned in previous work that using carbon black with an aqueous dispersing medium like exhibited a higher percolation threshold, due to the wettability of the dispersed medium [43].

4.2.1.3. Electrochemical impedance spectroscopy

The electrochemical impedance spectroscopy (EIS) is a sensitive technique to monitor the development of microstructure in dispersions at equilibrium. The electrical resistivity of the dispersion (and hence the electrical conductivity) expresses the degree of aggregation of KB particles, i.e., the extent of conductive pathways in the dispersions. Accordingly, the dependency of electrical conductivity (Σ) of dispersions on the carbon content confers deep insight on the microstructure evolution in the KB dispersions at equilibrium (non-flow conditions). Figure 6 shows impedance spectra, for various KB dispersions, represented by Nyquist plots. The diluted dispersions present nearly linear Nyquist plots (Fig. 6a) implying that the dispersions are not structured, and the ionic conductivity is dominant up to 0.7 wt% KB and the electrolyte is not electrically conductive.

At KB ≥ 0.9 wt%, the Nyquist plot is dominant by semicircle and linear tail as depicted in Fig. 6b. It is worth noting that the semicircle gets narrower as the KB content increases. This behavior can be ascribed to construction and growth of the conductive network in the dispersions. The EIS data can be quantitively represented by extrapolating the electrical conductivity when Nyquist plots are fitted by the equivalent circuit depicted in the inset Fig. 6b. This the optimal circuit that could be used to fit the impedance spectra of KB dispersions. The circuit is importantly composed of electronic resistor (R2) in series with non-ideal capacitive element (Q2). The result fitting parameter (R2 values) was used to calculate the electrical conductivity values of

dispersion, considering the geometrical parameter (plate diameter = 25 mm, gap = 1 mm). As shown in Fig. 5, the electrical conductivity monotonically increases with KB content until 2.1 wt% KB showing a scaling behavior with an exponent of 1.3. Above 2.1 wt% KB, the conductivity steeply increases with the KB content showing a higher exponent of 13 [51]. This carbon content is considered as saturation concentration above which denser network is formed as a result of numerous conductive pathways continuously grow as the KB content increase. This behavior causes abrupt increase in the electrical conductivity whereas the plateau modulus (G_0) remains nearly constant (Fig. 5).

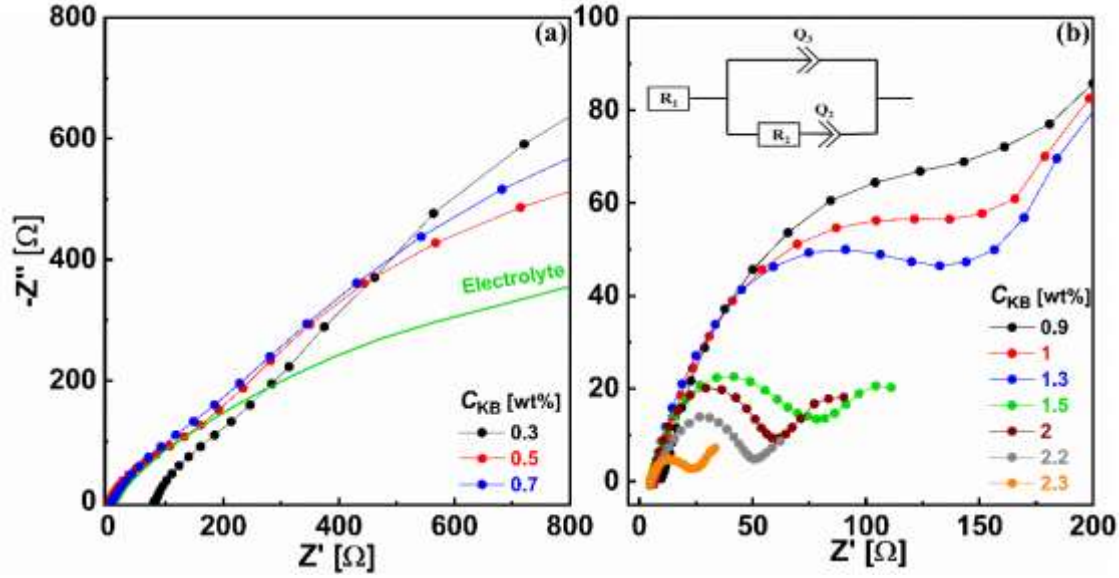

Figure 6 Impedance spectra expressed by Nyquist plots (*Z''*; imaginary part of impedance versus the real part *Z*') for (a) diluted and (b) concentrated KB dispersions at 25 ℃. The inset in (b) is the equivalent circuit.

Moreover, it is notably mentioned the KB dispersions begin to electrically percolate at 0.9 wt%; three times higher than the rheological percolating threshold as revealed from the behavior of G_0 (Fig. 5). Such variation between the rheological and electrical percolating thresholds (0.3 and 0.9 wt%, respectively) may ascribe to a peculiar microstructure evolution of carbon in this branched micelle solution. Presumably, the dispersions are rheologically percolated due to the formation of

anisometric KB aggregates that are long enough to interact during flow conferring the network elasticity. Nevertheless, the density number of conductive pathways has not been reached yet. The dispersions are electrically percolating when the effective pathways are numerous enough to link the aggregates and infinite network is formed [52]

4.2.1.4. Flow test

Steady-shear rheology (namely flow test) is a destructive test which elucidate the response of dispersions to the continuous shear flow. Since the electrode suspensions are exposed to continuous flow during its operation, this test is vital to explore any microstructural transition induced by flow. Figure 7 displays the variation of viscosity (η) with the applied shear rate ($\dot{\gamma}$) for selected examples of KB dispersions. Initially, the diluted dispersion at 0.2 wt% shows Newtonian behavior where η is nearly constant with ($\dot{\gamma}$). This indicates that the dispersion is not yet structured in accordance with the dynamic behavior where G'' is larger than G' (Fig. 4a). The semi–diluted dispersions at 0.3 and 0.5 wt% KB exhibit non-Newtonian behavior; namely shear–thinning (decrease of viscosity with shear rate). This behavior is likely to attribute to the breaking up of aggregates into smaller flocs that align with the flow and showing Newtonian behavior at higher shear rate (Fig. 7). Interestingly, the dispersions at 1.0 and 1.5 wt% KB reveal three-regime flow curve: two shear–thinning (at low and high $\dot{\gamma}$) separated by an intermediate viscosity plateau at moderate $\dot{\gamma}$. At low $\dot{\gamma}$, the KB network suffers shear–induced breaking up due to the rupture of carbon branches and aggregates are formed. These aggregates are likely to be anisometric enough to erode leading to the viscosity plateau (also increase in viscosity). At high $\dot{\gamma}$, the anisometric aggregates align in the flow direction showing the second shear–thinning behavior. The saturated dispersion at 2.1 wt% KB unusually shows a continuous shear–thinning

behavior over the whole range of $\dot{\gamma}$ without a distinct shear–thickening region (Fig. 7). This trend is likely to attribute to a breaking up of dense (saturated) network into smaller and nearly monodisperse flocs that are strongly interacting so that the thickening behavior is hidden. Similar behavior has been reported in previous study on the nonaqueous dispersions of carbon blacks [15].

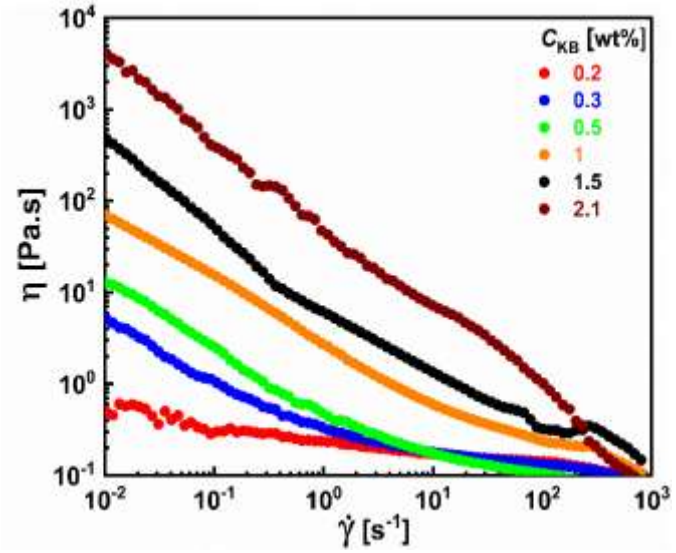

Figure 7 Variation of shear viscosity (η) with shear rate ($\dot{\gamma}$) for selected KB dispersions at 25 °C.

The simultaneous measurements of the impedance spectra under shear flow (rheo-electrical) for KB dispersions confer complementary evident for the shear–induced structural transitions as described aforementioned. Figure 8 demonstrates the dependency of electrical conductivity on the shear rate for two KB dispersions in the percolating regime (1 wt% KB) and at the onset of saturation (2.1 wt% KB). The electrical conductivity of the percolated dispersion at 1 wt% KB is independent of the shear rate until 20 s^{-1} (Fig. 8a). This trend is mainly due to the interacting anisometric aggregates that retain the dispersion yet conductive. Above 20 s^{-1} the aggregates get smaller so that the conductivity drops before it returns to increase above 100 s^{-1} in tandem with the thickening behavior (Fig. 7) explaining the interaction (erosion) between smaller flocs. On the other hand, the saturated dispersion at 2.1 wt% KB (Fig.

8b) exhibits a decrease of the electrical conductivity under flow until 50 s^{-1} as a result of the breaking up of the network. At higher $\dot{\gamma}$, the electrical conductivity strongly drops due to the formation of smaller flocs that are unable to retain the electrical conductivity of dispersion.

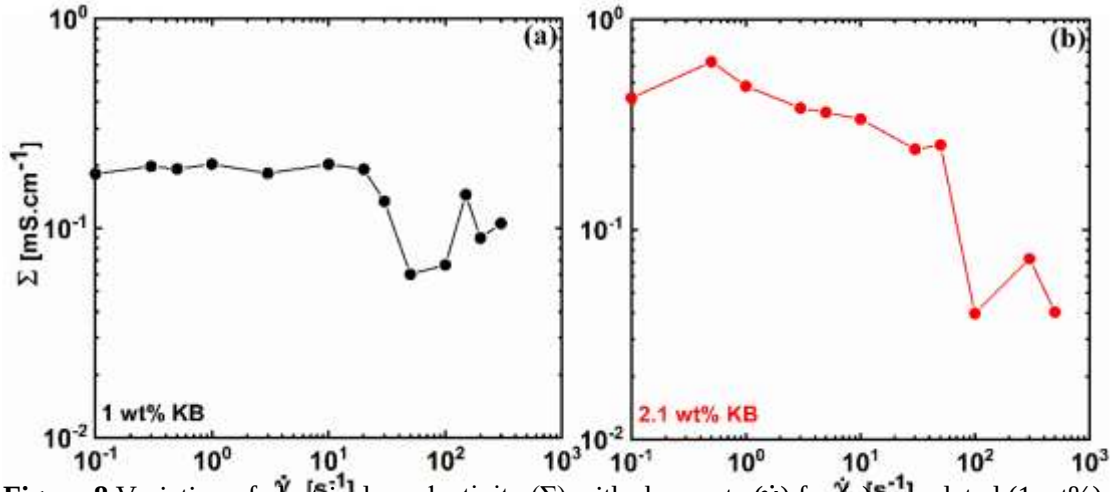

Figure 8 Variation of electrical conductivity (Σ) with shear rate ($\dot{\gamma}$) for (a) percolated (1 wt%) and (b) saturated (2.1 wt%) KB dispersions at 25 °C.

To recap, the dispersions of KB in branched micelle solution is rheologically percolated (i.e., three–dimensionally structured) at relatively low threshold (0.3 wt%) indicating the excellent wettability of the dispersing medium. Accordingly, the dispersion is electrically percolated at 0.9 wt%. Therefore, two KB concentrations (namely, 1.5 and 2.1 wt%) have been selected as conductive additives in the formulation of anolytes.

5.1. Synthesis and characterization of sodium titanate

The dry ball–mill method has been reported as an optimal approach to synthesize sodium titanates without the implications accompany the solvent–based methods such as hydrothermal method [40]. The crystalline structure and purity of the as-synthesized sodium titanate (as detailed in Section 3.3) have been examined by Raman spectroscopy and X-ray diffraction (XRD). The Raman spectrum of the as-synthesized material (Fig. 9a) is dominant by featured modes at *ca.* 304, 342, 486, 656,

849 and 882 cm^{-1} which are characteristic modes for layered $Na_2Ti_3O_7$ phase in agreement with previous reports [40, 53]. Traces of $Na_2Ti_6O_{13}$ structure may exist as indicated from the modes at 224 and 278 cm^{-1}. Moreover, no modes have been shown for unreacted precursor materials (TiO_2 anatase and Na_2CO_3).

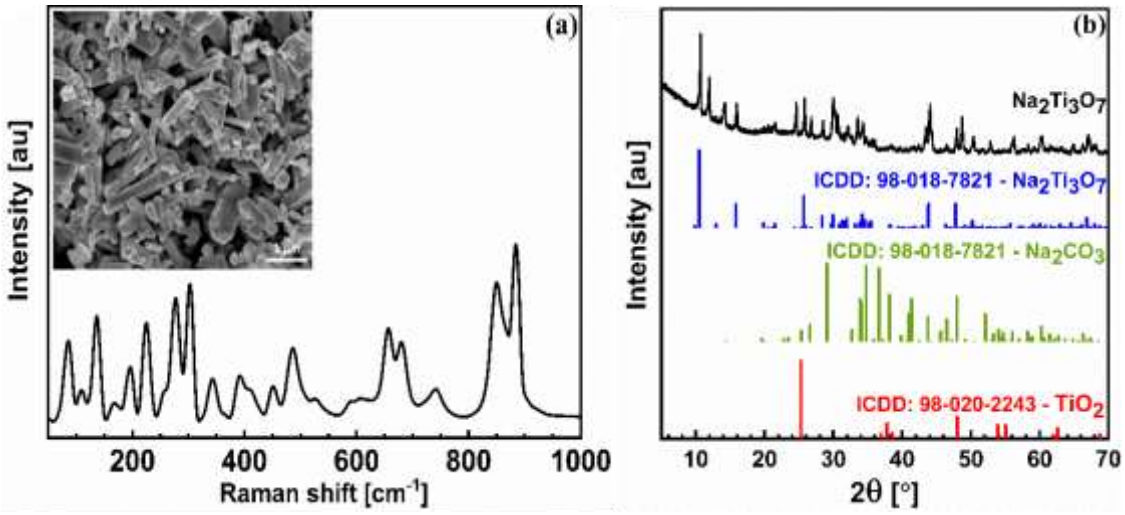

Figure 9 (a) Raman spectrum of the as-synthesized $Na_2Ti_3O_7$. The inset is the scanning electron micrograph of NTO (scale bar is 1 μm), (b) XRD diffraction pattern of $Na_2Ti_3O_7$. The colored lines are the reference diffraction lines for the synthesized $Na_2Ti_3O_7$, and precursor materials (TiO_2 anatase and Na_2CO_3 anhydrous).

Figure 9b displays the XRD diffraction pattern of the as-synthesized material and the reference lines for $Na_2Ti_3O_7$ and precursor materials. No diffraction peaks of unreacted starting materials have been detected implying the reaction completion and formation of sodium titanate. The pattern is consistent with that of the reference $Na_2T_3O_7$ (ICDD: 98-018-7821) with characteristic peaks at $2\theta = 10.7^\circ$ (100), 16° (101), 25.8° (110), and 44° (104). Other diffraction peaks (at $2\theta = 12^\circ$, 14°, 26.6°) are observed in the pattern indicating the coexistence of trace amount of $Na_2Ti_6O_{13}$ in agreement with the Raman spectrum. The morphology of the as-synthesized material is examined by SEM as depicted in the micrograph in the inset of Fig. 9a. The material is

polydisperse nanorods with an average length of *ca*. 700 nm–1.1 μm and width of few hundred nanometres.

6.1. Formulation and characterization of the flowable anolyte

To the percolated KB dispersion(s), we attempt to formulate and characterize flowable anolytes with maximum loading of electrochemical active material. Sodium titanate (NTO) has been chosen as anode material due to its relatively high theoretical capacity (*ca.* 178 mAh g^{-1}) and low working potential [11]. The anolytes are formulated through a gradual (systematic) addition of NTO to the percolated KB dispersion and examined rheologically and electrically. The optimal anolytes are those with optimal rheological (flowable) and electrical (yet conductive) under flow conditions at highest NTO content.

6.1.2. Equilibrium microstructure of anolytes (static mode)

Electrode suspension is composed of solid materials (conductive additive (KB) and active material (NTO)) dispersed in an electrolyte (branched micelle solution). It has been shown that the aqueous dispersion of KB is rheologically and electrically percolated at KB ≥ 0.9 wt%. Here, a network of carbon aggregates connected by pathways is constructed (inset of Fig. 5). Upon adding the electrically–insulated active material, breaking up of the conductive network or even pathway rupturing may takes place. This certainly results in serious loss of the electrical conductivity of anolyte rather than undesired increase in the rigidity of the suspension. Accordingly, it is rational to assess the influence of sodium titanate (NTO) content on the microstructure of anolytes made up of KB and NTO dispersed in branched micelle solution to find out the optimal composition of NTO at which the electrode suspension is somewhat flowable and yet electrically conductive. In other words, to what extend (content of

NTO) the percolated KB dispersion can sustain highest amount of NTO without serious loss of electrically conductivity and increased elasticity under equilibrium conditions?

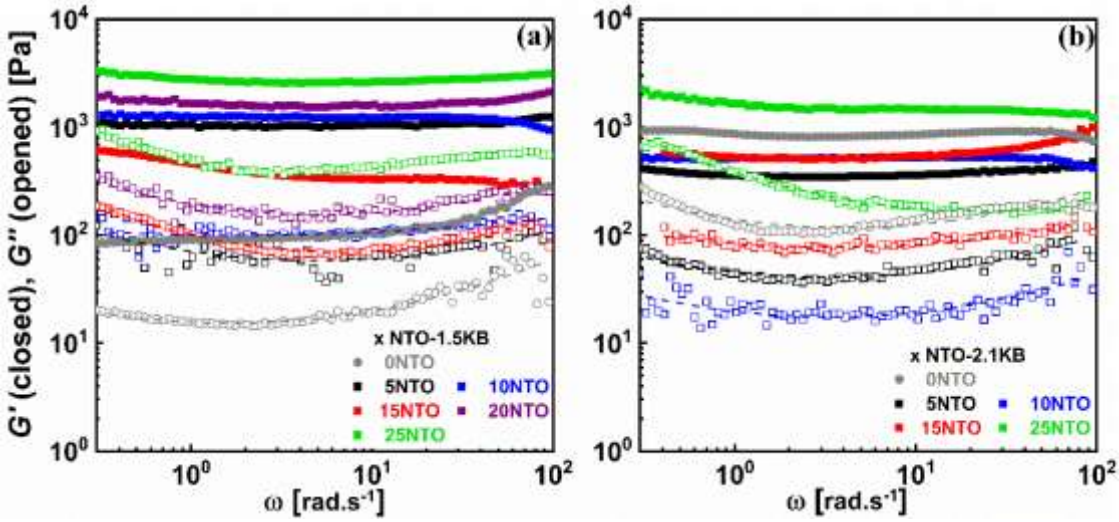

Figure 10 Frequency sweep rheograms of NTO–KB anolytes at (a) 1.5 and (b) 2.1 wt% KB at 25 °C. The dynamic measurements have been done at γ = 0.1%. x denotes the content of NTO in wt%. The dashed lines are guide for eyes.

In comparison, KB dispersions in the percolation regime (1.5 wt% KB) and at the saturation onset (2.1 wt% KB) have been selected to examine the effect of added NTO on the microstructure (rheologically and electrically) of the resultant anolytes at rest. Figure 10 demonstrates the dynamic frequency sweep results for the two types of anolytes in the linear regime (minimal perturbation at γ= 0.1%). For the anolytes formulated at 1.5 wt% KB, the suspensions commonly behave gel–like where G' is one–decade larger than G'' over the entire frequency range (Fig. 10a). It is worth noting the effect of NTO content on the dependency of G'' on the frequency.

As NTO content increases from 5 to 20 wt%, G'' becomes more dependent on the frequency. Similar dependency of the loss modulus has been reported in analogous suspensions [35]. This trend may ascribe to the reorganization of the carbon aggregates followed by breaking up of the weak pathways without significant influence on the rigidity of the suspensions [54]. At NTO ≥ 25 wt%, the suspensions turn stronger gel-like as revealed from the smaller difference (less than one decade) and weaker

dependency of the dynamic moduli on the frequency (see suspension at 25NTO-1.5KB in Fig. 10a). The electrical behavior of NTO-1.5 KB suspensions are in excellent agreement with the dynamic properties as revealed from the impedance spectra depicted in Fig. 11a. Upon addition of NTO to the 1.5 wt% KB, the characteristic semi-circle of the conductive network becomes wider indicating the breaking up of the conductive pathways due to the added NTO particles that are embedded in the KB network. Moreover, no significant variation in the impedance spectra has been noted over the entire NTO content.

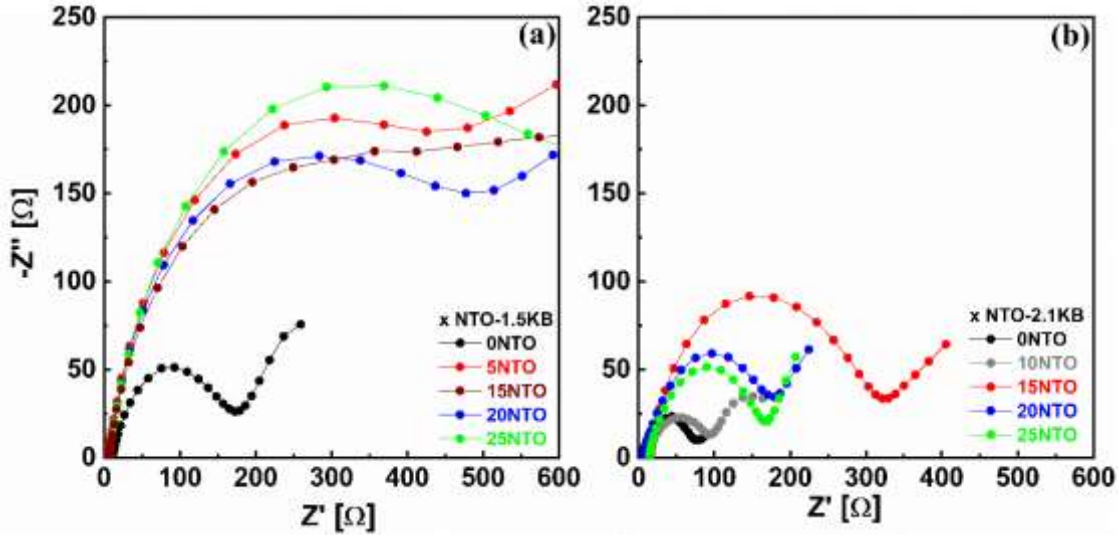

Figure 11 Nyquist plots of NTO–KB anolytes at (a) 1.5 and (b) 2.1 wt% KB at 25 ℃ (and 100 mV). x denotes the content of NTO in wt%.

On the other hand, the anolytes formulated in the saturated KB dispersion at 2.1 wt% similarly exhibit gel–like behavior over the studied NTO content (Fig. 10b). However, the dependency of G'' on the frequency is relatively weaker than that showed by analogous suspensions at 1.5 wt% KB. This implies the increased strength of network as a result of cooperative interaction between KB and NTO particles. The electrical behavior of NTO-2.1 KB suspensions supports this explanation where the semi-circles of Nyquist plots (Fig. 11b) strongly resemble that of the NTO-free KB

dispersion with nonmonotonic wider diameter as the NTO content rises.

Figure 12 quantitatively shows the influence of NTO content on the development of equilibrium microstructure of anolytes expressed by the rheological plateau modulus (G_0) and the electrical conductivity. On adding small amount of NTO (3 wt%) to the 1.5 wt% KB, G_0 strongly increases (one decade) in accordance with a small decrease in the conductivity (Fig. 12a).

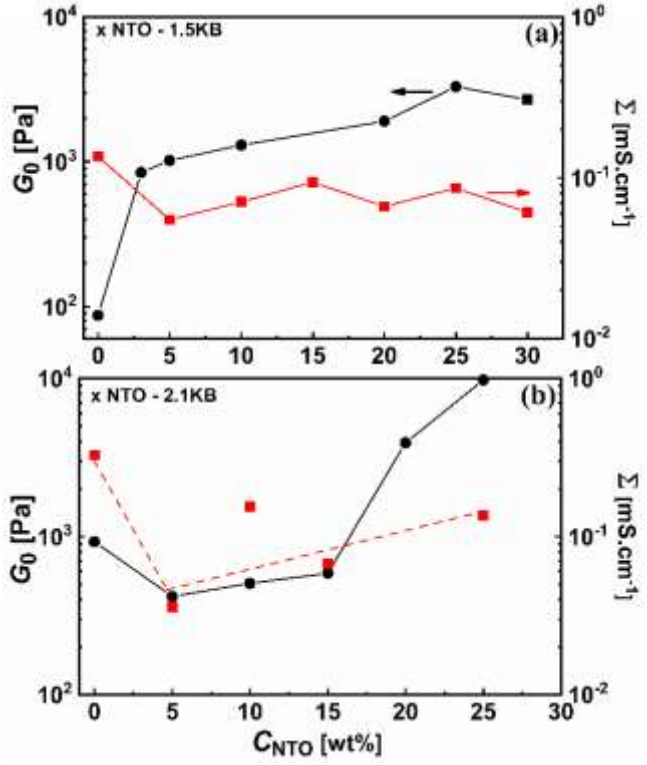

Figure 12 Effect of NTO content (C_{NTO}) on the plateau modulus (G_0) and electrical conductivity (Σ) of NTO–KB anolytes.

Further increase of NTO content does not significantly alter the network rigidity and electrical conductivity where G_0 and Σ remain nearly constant at higher NTO. This behavior may arise from the flexibility of the conductive network, rather than rupturing effect, at 1.5 wt% KB that can sustain higher load of NTO without significant decrease in the conductivity. On the other hand, G_0 of the saturated 2.1 wt% KB dispersion initially drops upon adding 5 wt% NTO and remains constant until 15 wt% NTO (Fig. 12b). Above this concentration, G_0 strongly increases. The initial drop

in G_0 is in tandem with a similar decrease in Σ at 5 wt% NTO, beyond which the conductivity of the anolytes does not significantly change at higher NTO content. This saturated dispersion is likely to sustain higher load of NTO, however, the network rigidity is enough high to be utilized as flowable anolyte. It is worth to mention that the anolyte at 30 wt% NTO is enough stiff to be examined by rheology.

Figure 13 displays the morphology and NTO distribution for a selected anolyte (10 wt% NTO–1.5 wt% KB). The optical micrograph demonstrates the homogenous distribution of the NTO particles in the KB conductive network (Fig. 13a). Deeper insight in the microstructure of the anolytes is gained from the SEM micrograph (Fig. 13b) which reveals the incorporation of the NTO nanorods in the KB network.

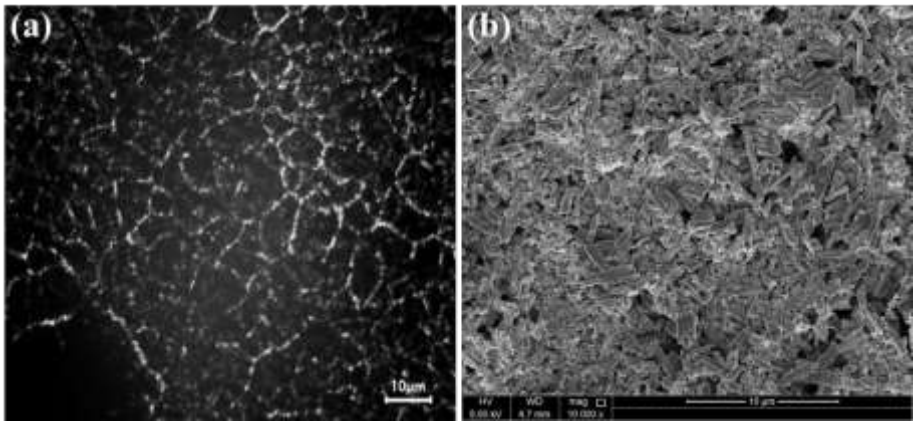

Figure 13 The morphology of selected anolyte (10NTO-1.5KB) (a) optical micrograph (scale bar = 10 μm), (b) SEM micrograph (scale bar = 10 μm).

6.1.3. Shear–induced structures (flow mode)

In general, NTO-KB anolytes commonly show non-Newtonian flow curves; shear–thinning behavior, where the viscosity (η) decreases with shear rate. Figure 14 depicts an example for two selected anolytes at 1.5 and 2.1 wt% KB and fixed NTO content (25 wt%). Interestingly, the anolyte (25NTO-1.5KB) shows a continuous shear–thinning behavior over the whole γ range without a distinct shear–thickening region (Fig. 14a). Nevertheless, the electrical conductivity (Σ) of (25NTO-1.5KB)

anolyte slightly decreases showing a minimum over intermediate shear rates (Fig. 14c). The decrease in η and Σ may arise from shear–induced structural transition in the KB network where the NTO particles weakens the networking tendency of the KB so that carbon branches and aggregates are formed at intermediate shear rate. At higher $\dot{\gamma}$, the electrical conductivity further decreases before it becomes constant at $\dot{\gamma} \geq 30\ s^{-1}$. The formation of smaller flocs that are unable to recover the electrical conductivity at high $\dot{\gamma}$ is likely to be the cause of this trend. This behavior may arise from the flexibility of the conductive KB network at 1.5 wt% that can sustain higher load of NTO (25 wt%) and keep the anolyte followable without significant decrease in Σ. On the other hand, the saturated dispersion at (25NTO-2.1KB) anolyte exhibits a decrease in η under flow as a result of the breaking up of the KB network (Fig. 14b). However, (25NTO-2.1KB) anolyte suspension shows an obvious change in η at moderate $\dot{\gamma}$ indicating that the embedded NTO nanorods in the saturated KB network produces a small aggregate with higher branch density which somewhat enhances the electrical conductivity (Fig. 14d). At high $\dot{\gamma}$, the electrical conductivity of (25NTO-2.1KB) significantly drops due to the formation of smaller flocs with lower density of branches that are unable to retain the conductivity under flow. It is worth to note that the 2.1 wt% KB network is stronger than 1.5 wt% KB network, therefore there was a fluctuating in the Σ at the whole range of $\dot{\gamma}$ and reveals the structural transition under flow. In analogous system (organic anolytes), similar shear-induced structural transition at critical active material has been reported [35]. The microstructure of this anolyte showed high sensitivity to $\dot{\gamma}$ where significant loss of electrical conductivity was observed. In comparison, the aqueous anolytes in this study, however, do not generally suffer strong loss in the conductivity owing mainly to the peculiar structure of dispersing medium (branched micelle solution).

In summary, the high NTO content in 1.5 wt% KB suspension does not significantly alter the network rigidity and electrical conductivity where Σ remain nearly constant at 25 wt% of NTO with the applied $\dot{\gamma}$. This behavior may arise from the flexibility of the conductive network in 1.5 wt% KB suspensions, rather than rupturing effect. However, the saturated 2.1 wt% KB with the same NTO content exhibited a significant decrease in the conductivity, indicating that rigid nature of the conductive network that are unable to sustain higher load of NTO nanorods.

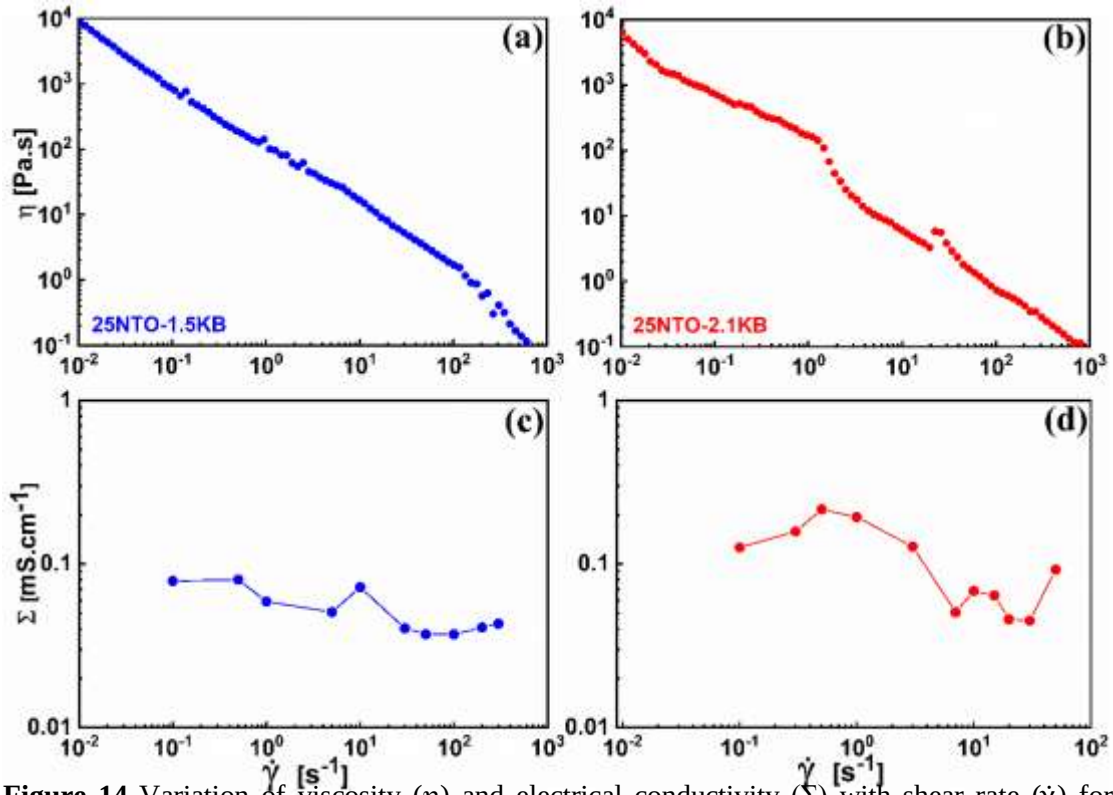

Figure 14 Variation of viscosity (η) and electrical conductivity (Σ) with shear rate ($\dot{\gamma}$) for selected anolytes (a,c) 25NTO-1.5KB and (b,d) saturated 25NTO-2.1KB at 25 °C. The conductivity values have been estimated after fitting the impedance spectra by the equivalent circuit (inset of Fig. 6b) as described in Section 4.2.1.3.

CHAPTER 4: CONCLUSION

Semi–solid flow battery (SSFB) is a promising grid energy storage system with scalable storage efficiency. For economic and environmental limitations, aqueous sodium semi–solid flow battery may offer an excellent alternative for the current conventional organic lithium – based flow batteries. The efficiency of SSFB can be enhanced by increasing the working potential of aqueous medium, optimize the formulation and select the optimal flow conditions at which the electrode suspensions operate. In the current study, we attempt to formulate and (rheologically and electrically) characterize the aqueous anolytes composed of carbon black (KB) and sodium titanate ($Na_2Ti_3O_7$; NTO) dispersed in branched micelle solution.

The branched micelle solution interestingly showed wide working potential of 2.59 V with relatively low viscosity at high concentration (1 M) of sodium salt. The compatibility between hydrophobic KB and the aqueous micelle solution is a key factor in controlling the aggregation mechanism and hence the microstructure of KB dispersions. While KB was rheologically percolated at 0.3 wt%, it begun to electrically percolate at 0.9 wt% forming a three-dimensional conductive network of aggregates connected by pathways. The high degree of pathways flexibility empowered these unique KB dispersions the ability to retain the electrical conductivity under flow conditions.

To examine the approach of dispersions in micelle solution, NTO–based anolytes showed varied rheological and electrical behaviours depending on the KB content. The anolytes formulated in the percolated 1.5 wt% KB dispersion could sustain higher load of sodium titanate (25 wt%) without significant effect on the rigidity and conductivity of the anolyte under static and flow modes. Whereas the anolytes formulated in saturated KB dispersions exhibited a significant decrease in the conductivity and could not sustain higher load of NTO nanorods.

CHAPTER 5: FUTURE WORK

Based on the current findings, a plan of future is as follows:

1. The evolution of microstructure of carbon dispersions and electrode suspensions will be examined microscopically under flow conditions. This will be done when the customized home-made shear cell is ready.

2. The electrochemical performance of optimal anolytes will be examined.

3. Sodium titanate has nanorod morphology with high aspect ratio which may negatively affect on the homogeneity of the electrode suspensions under flow. Accordingly, the density mismatching between NTO and KB should be minimized by grinding the NTO and decrease the particle size or convert them in semi-spherical particles for improved packing and hence compatibility in the suspension.

4. This branched micelle solution (as dispersing medium) will be used to formulate and characterize catholytes, following the same approach.

REFERENCES

1. Larcher, D. and J.-M. Tarascon, *Towards greener and more sustainable batteries for electrical energy storage.* Nature chemistry, 2015. **7**(1): p. 19-29.
2. Chen, H., et al., *Progress in electrical energy storage system: A critical review*. Progress in natural science, 2009. **19**(3): p. 291-312.
3. Krill III, C., H. Ehrhardt, and R. Birringer, *Thermodynamic stabilization of nanocrystallinity.* Zeitschrift für Metallkunde, 2005. **96**(10): p. 1134-1141.
4. Jeon, S.-i., et al., *Desalination via a new membrane capacitive deionization process utilizing flow-electrodes.* Energy & Environmental Science, 2013. **6**(5): p. 1471-1475.
5. Presser, V., et al., *The electrochemical flow capacitor: A new concept for rapid energy storage and recovery.* Advanced Energy Materials, 2012. **2**(7): p. 895-902.
6. Duduta, M., et al., *Semi-solid lithium rechargeable flow battery.* Advanced Energy Materials, 2011. **1**(4): p. 511-516.
7. Cho, I., et al., *A comparative investigation of carbon black (Super-P) and vapor-grown carbon fibers (VGCFs) as conductive additives for lithium-ion battery cathodes.* Rsc Advances, 2015. **5**(115): p. 95073-95078.
8. Notter, D.A., et al., *Contribution of Li-ion batteries to the environmental impact of electric vehicles*. 2010, ACS Publications.
9. Li, Z., et al., *Aqueous semi-solid flow cell: demonstration and analysis.* Physical Chemistry Chemical Physics, 2013. **15**(38): p. 15833-15839.
10. Yao, F., D.T. Pham, and Y.H. Lee, *Carbon-based materials for lithium-ion batteries, electrochemical capacitors, and their hybrid devices.* ChemSusChem, 2015. **8**(14): p. 2284-2311.

11. Ellis, B.L. and L.F. Nazar, *Sodium and sodium-ion energy storage batteries.* Current Opinion in Solid State and Materials Science, 2012. **16**(4): p. 168-177.
12. Brilloni, A., et al., *Improving the Electrical Percolating Network of Carbonaceous Slurries by Superconcentrated Electrolytes: An Electrochemical Impedance Spectroscopy Study.* ACS applied materials & interfaces, 2021. **13**(11): p. 13872-13882.
13. Lee, J., et al., *Use of surfactants for continuous operation of aqueous electrochemical flow capacitors.* Energy Technology, 2016. **4**(1): p. 75-84.
14. Madec, L., et al., *Surfactant for enhanced rheological, electrical, and electrochemical performance of suspensions for semisolid redox flow batteries and supercapacitors.* ChemPlusChem, 2015. **80**(2): p. 396-401.
15. Youssry, M., et al., *Non-aqueous carbon black suspensions for lithium-based redox flow batteries: rheology and simultaneous rheo-electrical behavior.* Physical Chemistry Chemical Physics, 2013. **15**(34): p. 14476-14486.
16. Narayanan, A., F. Mugele, and M.H. Duits, *Mechanical history dependence in carbon black suspensions for flow batteries: A rheo-impedance study.* Langmuir, 2017. **33**(7): p. 1629-1638.
17. Akuzum, B., et al., *Percolation characteristics of conductive additives for capacitive flowable (semi-solid) electrodes.* ACS applied materials & interfaces, 2020. **12**(5): p. 5866-5875.
18. Yang, S., et al., *Plate-shaped graphite for improved performance of flow-electrode capacitive deionization.* Journal of The Electrochemical Society, 2017. **164**(13): p. E480.
19. Yoon, H., et al., *Pseudocapacitive slurry electrodes using redox-active quinone for high-performance flow capacitors: an atomic-level understanding*

of pore texture and capacitance enhancement. Journal of Materials Chemistry A, 2015. **3**(46): p. 23323-23332.

20. Yang, S., et al., *Flow-electrode capacitive deionization using an aqueous electrolyte with a high salt concentration.* Environmental science & technology, 2016. **50**(11): p. 5892-5899.

21. Kim, K.M., et al., *Effect of mixing sequences on the electrode characteristics of lithium-ion rechargeable batteries.* Journal of power sources, 1999. **83**(1-2): p. 108-113.

22. Zhang, W., et al., *Effect of slurry preparation and dispersion on electrochemical performances of LiFePO 4 composite electrode.* Ionics, 2011. **17**(5): p. 473-477.

23. Zhang, Q., et al., *Nanomaterials for energy conversion and storage.* Chemical Society Reviews, 2013. **42**(7): p. 3127-3171.

24. Amari, T. and K. Watanabe, *Flow properties and electrical conductivity of carbon black–linseed oil suspension.* Journal of Rheology, 1990. **34**(2): p. 207-221.

25. Genovese, D.B., *Shear rheology of hard-sphere, dispersed, and aggregated suspensions, and filler-matrix composites.* Advances in colloid and interface science, 2012. **171**: p. 1-16.

26. Kinloch, I.A., S.A. Roberts, and A.H. Windle, *A rheological study of concentrated aqueous nanotube dispersions.* Polymer, 2002. **43**(26): p. 7483-7491.

27. Zhao, Y. and H.R. Byon, *High-performance lithium-iodine flow battery.* Advanced Energy Materials, 2013. **3**(12): p. 1630-1635.

28. Weber, A.Z., et al., *Redox flow batteries: a review.* Journal of applied electrochemistry, 2011. **41**(10): p. 1137.

29. Zhen, Y. and Y. Li, *Redox flow battery*, in *Studies in Surface Science and Catalysis*. 2019, Elsevier. p. 385-413.

30. Zhao, Y., et al., *A chemistry and material perspective on lithium redox flow batteries towards high-density electrical energy storage.* Chemical Society Reviews, 2015. **44**(22): p. 7968-7996.

31. Soloveichik, G.L., *Flow batteries: current status and trends.* Chemical reviews, 2015. **115**(20): p. 11533-11558.

32. Leung, P. and X. Li, *CP de. Leon, L. Berlouis, CT John Low and FC Walsh.* RSC Adv, 2012. **2**: p. 10125.

33. Hamelet, S., et al., *Silicon-based non aqueous anolyte for Li redox-flow batteries.* Journal of The Electrochemical Society, 2013. **160**(3): p. A516.

34. Park, M., et al., *Material design and engineering of next-generation flow-battery technologies.* Nature Reviews Materials, 2016. **2**(1): p. 1-18.

35. Youssry, M., et al., *Formulation of flowable anolyte for redox flow batteries: Rheo-electrical study.* Journal of Power Sources, 2015. **274**: p. 424-431.

36. Darling, R.M., et al., *Pathways to low-cost electrochemical energy storage: a comparison of aqueous and nonaqueous flow batteries.* Energy & Environmental Science, 2014. **7**(11): p. 3459-3477.

37. Chayambuka, K., J. Fransaer, and X. Dominguez-Benetton, *Modeling and design of semi-solid flow batteries.* Journal of Power Sources, 2019. **434**: p. 226740.

38. Wu, C., et al., *Design and Synthesis of Layered Na2Ti3O7 and Tunnel Na2Ti6O13 Hybrid Structures with Enhanced Electrochemical Behavior for Sodium-Ion Batteries.* Advanced science, 2018. **5**(9): p. 1800519.

39. Ventosa, E., O. Amedu, and W. Schuhmann, *Aqueous mixed-cation semi-solid hybrid-flow batteries.* ACS Applied Energy Materials, 2018. **1**(10): p. 5158-5162.

40. Youssry, M. and A. Mussa, *Controllable synthesis of sodium titanates using facile ball milling method.* Ceramics International, 2021. **47**(10): p. 14021-14032.

41. Wu, S. and H. Mohammadigoushki, *Linear versus branched: flow of a wormlike micellar fluid past a falling sphere.* Soft Matter, 2021. **17**(16): p. 4395-4406.

42. Tomiyasu, H., et al., *An aqueous electrolyte of the widest potential window and its superior capability for capacitors.* Scientific reports, 2017. **7**(1): p. 1-12.

43. Youssry, M., et al., *Aqueous dispersions of carbon black and its hybrid with carbon nanofibers.* RSC advances, 2018. **8**(56): p. 32119-32131.

44. Vallés, C., et al., *The rheological behaviour of concentrated dispersions of graphene oxide.* Journal of Materials Science, 2014. **49**(18): p. 6311-6320.

45. Yearsley, K.M., et al., *The rheology of multiwalled carbon nanotube and carbon black suspensions.* Journal of Rheology, 2012. **56**(6): p. 1465-1490.

46. Piao, S.H., et al., *Dispersion state and rheological characteristics of carbon nanotube suspensions.* Journal of industrial and engineering chemistry, 2017. **52**: p. 369-375.

47. Mills, P., J. Goodwin, and B. Grover, *Shear field modification of strongly flocculated suspensions—aggregate morphology.* Colloid and Polymer Science, 1991. **269**(9): p. 949-963.

48. Tadros, T.F., *Rheology of dispersions: principles and applications*. 2011: John Wiley & Sons.

49. Trappe, V. and D. Weitz, *Scaling of the viscoelasticity of weakly attractive particles.* Physical review letters, 2000. **85**(2): p. 449.

50. Aoki, Y., A. Hatano, and H. Watanabe, *Rheology of carbon black suspensions. II. Well dispersed system.* Rheologica acta, 2003. **42**(4): p. 321-325.

51. Stauffer, D. and A. Aharony, *Introduction to percolation theory*. 2018: CRC press.

52. Penu, C., et al., *Rheological and electrical percolation thresholds of carbon nanotube/polymer nanocomposites.* Polymer Engineering & Science, 2012. **52**(10): p. 2173-2181.

53. Bamberger, C.E. and G.M. Begun, *Sodium titanates: stoichiometry and Raman spectra.* Journal of the American Ceramic Society, 1987. **70**(3): p. C-48-C-51.

54. Mongondry, P., C.W. Macosko, and T. Moaddel, *Rheology of highly concentrated anionic surfactants.* Rheologica acta, 2006. **45**(6): p. 891-898.